Secondary Phases Quantification and Fracture Toughness at Cryogenic Temperature of Austenitic Stainless Steel Welds for High-Field Superconducting Magnets

Ignacio Aviles Santillana, Pilar Fernandez Pison, Stefanie Agnes Elisabeth Langeslag, Stefano Sgobba, Alexander Lunt, Christelle Boyer, and Elisa Maria Ruiz Navas

***Abstract*—The ITER magnet system is based on the "cable-in-conduit" conductor concept, which consists of various types of stainless steel jackets filled with superconducting strands. The jackets provide high strength and fracture toughness to counteract the high stress imposed by, amongst others, electromagnetic loads at cryogenic temperature. Material properties of austenitic stainless steel at cryogenic temperature are known to some extent, but only partial information is available for their welds, particularly in combination with weld fillers envisaged for cryogenic service. When a full inspection of the welded components is not possible, it becomes of special interest an assessment of its fracture toughness under close-to-service conditions if a fracture mechanics' design approach is to be adopted. In absence of defects, brittle secondary phases are generally held responsible of the loss of ductility and toughness which is to be expected after postweld heat treatments. Their quantification becomes thus essential in order to explain the negative impact in fracture toughness after unavoidable thermal treatments. This paper investigates fracture toughness behavior at 7 K of AISI 316L and AISI 316LN tungsten inert gas welds using two fillers adapted to cryogenic service, EN 1.4453 and JK2LB. Additionally, the effect of such an aforementioned heat treatment, here the Nb_3Sn reaction heat treatment (650° for 200 h) on fracture toughness of the welds is evaluated. A correlation between the evolution of properties and the quantity of secondary phases as a result of the above treatment is provided.**

***Index Terms*—Fracture toughness, austenitic stainless steel welds, cryogenic, secondary phases.**

I. Introduction

THE iter tokamak requires a superconducting magnet system in order to form, control, shape and drive the plasma.

Manuscript received September 15, 2017; accepted February 12, 2018. Date of publication February 27, 2018; date of current version April 6, 2018. *(Corresponding author: Ignacio Aviles Santillana.)*

I. A. Santillana and P. F. Pison are with CERN, Geneva 1211, Switzerland, and also with the University Carlos III of Madrid, Leganes 28911, Spain (e-mail: Ignacio.aviles.santillana@cern.ch).

S. A. E. Langeslag, S. Sgobba, and A. Lunt are with CERN, Geneva 1211, Switzerland.

C. Boyer is with the ITER Organization, St. Paul Lez Durance 13115, France (e-mail: Christelle.boyer@iter.org).

E. M. R. Navas is with the University Carlos III of Madrid, Leganes 28911, Spain (e-mail: emruiz@ing.uc3m.es).

Color versions of one or more of the figures in this paper are available online at http://ieeexplore.ieee.org.

Digital Object Identifier 10.1109/TASC.2018.2809481

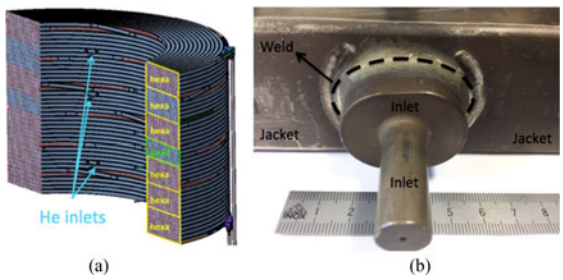

Fig. 1. (a) CS module (110 tons, 2.1 m height, 4.1 m diameter) displaying the positions of the He inlets (located at the inner radius) [3]. (b) CS He inlet mock – up welded to the jacket.

It is divided into four main sub-systems: 18 toroidal field (TF) coils; the central solenoid (CS); 6 poloidal field (PF) coils; and 9 pairs of correction coils (CCs) [1]. These superconducting magnets are cooled with supercritical helium at 4.2 K [1]. The high thermal contractions during cool down from 300 K to operation temperature together with the enormous Lorentz forces which are exerted will result in highly stressed components [2]. The ITER magnet system uses the concept of 'cable-in-conduit' conductors (CICC) consisting of superconducting strands inserted in austenitic stainless steel jackets, which act as structural components. For the transitions between them and for their joining to other components such as He inlets (Fig. 1) and outlets, Tungsten Inert Gas (TIG) welds are the baseline. To be able to withstand currents as high as 68 kA [2], CS and TF coils are manufactured out of Nb_3Sn strands, which after insertion in the circular cross section jacket, compaction and coiling, need to be submitted to the so – called reaction heat treatment (650 °C for 200 hours). This treatment, essential for the formation of the superconducting Nb_3Sn phase, has a strong impact on the mechanical properties at cryogenic temperature of the jackets and welds.

For this study, premium grades of AISI 316L and AISI 316LN were employed, coming from Electro Slag Remelted (ESR) slabs to reduce impurities and inclusions. For the filler materials, a commercial alloy (EN 1.4453, AWS ER317LN) and a high manganese alloy (JK2LB), both suited for cryogenic applications, were compared.

TABLE I
RESULTS OF FRACTURE TOUGHNESS FOR THE DIFFERENT SAMPLES

Sample designation	J_Q (kJ/m^2)	K_{JIC} (MPa$\sqrt{}$m)
L-4453-NHT	252 ± 10	238 ± 4
L-4453-HTR	78 ± 6	132 ± 5
LN-4453-NHT	345 ± 0	262 ± 0
LN-4453-HTR	107 ± 12	151 ± 12
LN-JK2LB-NHT	355 ± 4	266 ± 1
LN-JK2LB-HTR	269 ± 6	232 ± 3

II. EXPERIMENTAL

A. Welding and Heat Treatment

The weld plates were prepared based on an existing Welding Procedure Specification (WPS). The dimensions of the plates to be used as base material were chosen to fulfil standard ISO 15614.6 mm thick plates were welded and afterwards machined down to 4 mm by removing 1 mm from each side.

The joint is a full penetration butt weld (BW) with a flat position (Flat – PA) in a "V" configuration of 90°, welded from one side without backing. The process TIG with filler metal (142 according to ISO 4063), with an argon shielding. Welds were done in 3 passes, with the gas flow at 10 L/min. A negative polarity on the cathode and direct current was used in order to produce a narrow weld bead.

The heat treatment is performed under vacuum (10^{-6} mbar), with a heating ramp-up of 5 °C/hour followed by a plateau of 200 hours at 650 °C. Pieces are cooled via natural convection at approximately 30 °C/hour.

B. Fracture Toughness

12 compact tension (CT) specimens (Table I) with W = 36 mm, B = 4 mm and without side grooves (two per combination of base material, filler material and heat treatment) are machined from the mid part of the welded plates according to ASTM E1820-01. The notch tip of all specimens was in the middle of the weld bead. Crack propagation runs parallel to the weld axis, in longitudinal orientation (T-L orientation according to ASTM 1823). A naming convention has been established for the sample designation: the first part corresponds to the base material (L or LN); the second is a reference to the filler material (4453 or JK2LB); the last differentiates the samples which have been heat treated (HTR) with the ones which have not (NHT). All the measurements were conducted at 7 K in a temperature controlled cryostat.

Precracking was performed according to ASTM E1820 at a frequency of 15 Hz to avoid heating the specimen. An extensometer fixed at the load line of the CT specimen to follow the position of the crack tip both during precracking and during fracture testing.

The unloading compliance was afterwards used to obtain a J - Δa curve (resistance curve) from which the toughness values (J_Q) are obtained. Despite of the fact that the thickness criterion of ASTM E1820 is not fulfilled, the WPS was conceived to represent a welding procedure typical of the ITER magnet system (3 pass TIG weld of 4 mm thickness). A conversion to K_{JIC} is also presented for information since the technical specifications demand a minimum K_{IC}. However, the values herein contained are size dependent but are directly relevant for specific designs assuming that the specimen is identical in thickness to the intended service component.

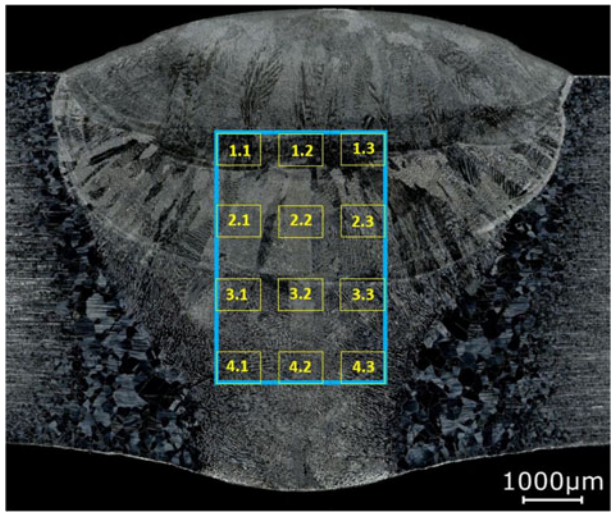

Fig. 2. Example of a weld's cross section showing the sampling routine performed for the assessment of secondary phases via image analysis. Each of the 12 squares represents a 3 × 3 matrix of images at 1000x magnification per individual image. Etching: Oxalic acid, 10% in volume, electrolytic.

C. Secondary Phase Quantification via SEM and Image Analysis

The brittleness at operating temperature of secondary phases different from austenite has an impact in the mechanical properties. By using a Scanning Electron Microscope (SEM), a cross section of each sample was analyzed using a backscattered electron detector. Since crack growth was observed to be confined into a 4 mm × 3 mm rectangle, this is the area which was scanned obtaining 1000× magnification individual images, which were afterwards put together. A systematic sampling of this surface was performed as shown in Fig. 2 for a total of 108 images analyzed per sample. Images were processed with a professional image analysis software that allows the discrimination of the different grey levels, which correspond to the different compositions and thus in our case, the different phases.

Additionally, in order to assess the morphology of the σ - phase in all spatial directions, a Focused Ion Beam (FIB) tomography has been performed on sample L-4453-HTR, consisting on a redundant backscattered electron imaging followed by a nanomachining layer by layer with the ion beam, what allows for a 3D reconstruction of the inspected volume.

D. Sensitization Testing

In addition to a potential loss of corrosion resistance induced by sensitization, the carbides can create a continuous network of brittle intermetallics at the grain boundaries which might have a negative impact in fracture toughness.

An assessment of the sensitization of all the samples was performed according to ASTM A262 practice A and practice

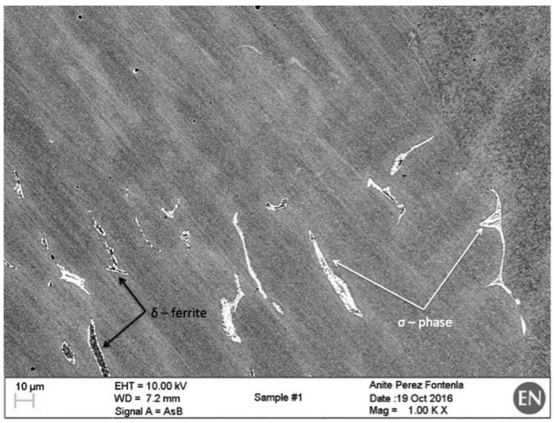

Fig. 3. Backscattered electron image of the weld bead of sample L-4453-NHT. Original magnification: 1000x. Sample was observed in as – polished state. Taken from position 4.2 (see Fig. 2). δ – ferrite and σ – phase are shown.

D, the latter being especially suitable for AISI 316 and AISI 317 austenitic stainless steel families. For this analysis, a parallelepipedic sample of 2 mm $\times$ 2 mm $\times$ 30 mm was extracted from the weld seam of each sample.

III. Results and Discussion

A. Fracture Toughness

The results extracted from the assessment of the J - Δa curves for each specimen together with the K_{JIC} values shown for information are displayed in Table I, where the average of the two specimens $\pm$ the associated statistical error is shown. The conversion from J_{IC} to K_{JIC} is performed following ASTM 1820 appendix A9. The required properties (E and ν) have been obtained from [4] and [5]. The negative effect of the reaction heat treatment in the fracture toughness at cryogenic temperature is noticed, as well as a higher fracture toughness of the samples using AISI 316LN as base material. When comparing the filler materials, JK2LB shows a higher fracture toughness at cryogenic temperature both in as welded state as well as a very high toughness after heat treatment.

B. Results of Secondary Phase Quantification via SEM and Image Analysis.

As it can be seen in Fig. 3, the contrast given by the different chemical composition of the secondary phases was used for their recognition and quantification via image analysis. δ – ferrite is darker with respect to the austenitic matrix due to its higher chromium and lower nickel content, whereas σ – phase corresponds to the brighter regions embedded in the grey austenitic matrix thanks to its higher Mo content.

The image analysis of 108 individual images of one cross section of each sample yields the results gathered in Table II. The area % represents the ratio between the area covered by each secondary phase and the total area analysed.

Based on the results shown in Table II, the amount of δ – ferrite and σ – phase is higher in the samples using AISI 316L as base material (for its equivalent sample using AISI 316LN), what is explained by a more favorable composition of the samples using AISI 316LN (N being an extremely powerful austenite stabilizer). It is also evident that no secondary phases are accounted for when the filler material employed is JK2LB. The low Mo content and the extremely low content of Cr (for an austenitic stainless steel) together with an extremely high content of manganese explains the scarce quantity of secondary phases which is observed for this filler material.

These results are in agreement with the hypothesis stating that a higher content of phases others than austenite would imply a poorer fracture toughness at cryogenic temperature [6]–[8].

The 3D reconstruction via FIB tomography reveals that sigma phase follows a plane diagonally across the gauge volume studied (Fig. 4) for the studied sample (L-4453-HTR). The sigma phase is not continuous over this region but is instead contained within small particles with diameter 0.3–3 μm. The results of this analysis therefore suggest that the sigma phase contained within this region of austenitic stainless steel TIG weld has a preferential form which is of microscale particles or planes with dimensions in the range 0.3–3 μm.

TABLE II
Secondary Phase Quantification of the Backscattered Electron SEM Images via Image Analysis for the Different Samples

Sample designation	δ – ferrite (area %)	σ – phase (area %)
L-4453-NHT	0.28	0.17
L-4453-HTR	0.13	0.42
LN-4453-NHT	0.01	0.03
LN-4453-HTR	0.00	0.13
LN-JK2LB-NHT	0.00	0.00
LN-JK2LB-HTR	0.00	0.00

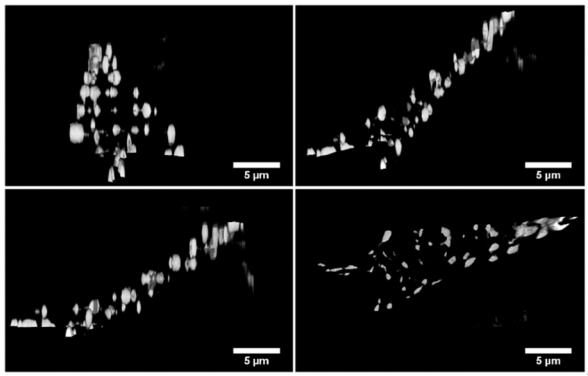

Fig. 4. 3D reconstruction of the sigma phase of the weld bead of sample L-4453-HTR using backscattered electron image combined with Focused Ion Beam (FIB) nanomachining. The Z axis runs parallel to the direction of the weld. Taken from position 4.1 (see Fig. 2).

C. Results of Sensitization Testing

A screening of one cross section of all samples was performed according to ASTM A262 practice A in order to classify their sensitization structures. All the results are displayed in Table III, that also shows the rate of corrosion (ROC) of all the analyzed samples after applying ASTM A262 practice D. This practice is used as a semi-quantitative value for a comparative assessment of the presence of carbides at the grain boundaries.

TABLE III
SENSITIZATION STRUCTURE AND RATE OF CORROSION (ROC) FOR EACH OF THE SAMPLES ANALYZED AFTER ASTM A262 PRACTICE A AND PRACTICE D WERE APPLIED

Sample designation	Sensitization structure	Rate of corrosion (μm/h)
L-4453-NHT	Dual	11.6
L-4453-HTR	Ditch	12.6
LN-4453-NHT	Step	5.8
LN-4453-HTR	Dual	6.8
LN-JK2LB-NHT	Step	178.8
LN-JK2LB-HTR	Dual	179.5

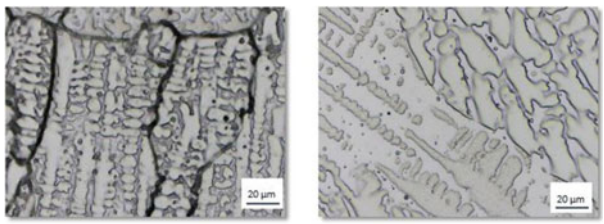

Fig. 5. Sensitization structures after ASTM-A262 method A. Original magnification: 500x. (a) Sample L-4453-HTR. Ditch structure. (b) Sample LN-4453-NHT. Step structure.

Taking into account the degree of severity of the sensitization structures (Ditch $>$ Dual $>$ Step), based on the results shown in Table III and Fig. 5, the material is systematically more sensitized after heat treatment, something to be expected in this temperature range [9]. It is also evident a more favorable behavior towards sensitization when AISI 316LN is used as base material.

When analyzing the rates of corrosion obtained using ASTM A262 practice D, it is once again clear that the samples are more sensitized after the reaction heat treatment. Putting the focus on the samples using EN 1.4453 as filler material, it becomes evident that samples using AISI 316LN as base material are less sensitized than the ones using AISI 316L. However, an extremely high ROC is observed for both samples using JK2LB as filler material. A generalized corrosion of this material due to its widely different composition makes it unsuitable for an assessment of its ROC using ASTM A262 practice D.

Based on the sensitization testing results with the screening practice of ASTM A262, the least severe sensitization structure (step) corresponds to a much higher fracture toughness at cryogenic temperature. Intermediate values of toughness are found for the 'dual' structure. The poorest value of fracture toughness corresponds to the most critical sensitization structure (ditch).

Being practice D of ASTM A262 specially conceived for AISI 316 and AISI 317 austenitic stainless steel families, the abnormal ROCs measured for samples employing JK2LB as filler material are attributed to the very different composition of this filler with respect to the mentioned austenitic stainless steel families. The generalized corrosion occurring makes it impossible to assess its sensitization using this practice.

IV. FINAL REMARKS AND CONCLUSIONS

The present work shows exploitable values of fracture toughness at cryogenic temperature of austenitic stainless steel TIG welds in the range of 4 mm thickness. Various filler metals are studied and the impact of the reaction heat treatment has been assessed.

The pernicious effect of micrometric secondary phases (δ – ferrite and σ – phase) to the cryogenic fracture toughness is highlighted, as it was previously observed in In order to obtain a better correlation, aspects such as the inclusion content and the morphology and distribution of the secondary phases should be addressed, as suggested by [7].

For the smaller secondary phases (carbides), the corrosion studies carried out show a good agreement between the rates of corrosion and the mechanical performance of the samples when AISI 316 and 317 austenitic stainless steel families are assessed. For other compositions, other methods should be found. On the other hand, the screening method shows a fairly good correlation between the severity of the sensitization structures and the fracture toughness at cryogenic temperature.

Bearing in mind the challenges that implies fracture toughness at cryogenic temperature testing, a suggested sensitive approach consists of a first screening via quantification of secondary phases to only test the ones showing low quantities of brittle phases: step or dual sensitization structure according to ASTM A262 method A and less than 0.5 % area percentage of δ – ferrite + σ – phase.

ACKNOWLEDGMENT

The authors would like to thank A.T. P. Fontenla for her help with the SEM imaging and B. Teissandier for his help with the sensitization testing.

REFERENCES

[1] C. Sborchia *et al.*, "Overview of ITER magnet system and European contribution," in *Proc. 2011 IEEE/NPSS 24th Symp. Fusion Eng.*, 2011, pp. 1–8.
[2] N. Mitchell, A. Devred, P. Libeyre, B. Lim, and F. Savary, "The ITER mag¬nets: Design and construction status," *IEEE Trans. Appl. Supercond.*, vol. 22, no. 3, Jun. 2012, Art. no. 4200809.
[3] G. Rolando, A. Devred, and A. Nijhuis, "Temperature and current margin of ITER central solenoid conductor designs during a 15 MA plasma scenario," *Supercond. Sci. Technol.*, vol. 27, no. 2, 2013, Art. no. 025010.
[4] H. M. Ledbetter, W. F. Weston, and E. R. Naimon, "Low-temperature elastic properties of four austenitic stainless steels," *J. Appl. Phys.*, vol. 46, no. 9, pp. 3855–3860, 1975.
[5] K. Hamada, "Tensile properties of JK2LB at cryogenic temperature," Internal communication, unpublished.
[6] D. T. Read, H. I. McHenry, P. Steinmeyer, and R. D. Thomas, Jr., "Metallurgical factors affecting the toughness of 316 L SMA weldments at cryogenic temperatures," *Welding J.*, vol. 59, no. 4, p. 104, 1980.
[7] J. W. Morris, "Steels for low temperature applications," in *Encyclopedia of Advanced Materials*, Rep. no. LBL-34968, 1993.
[8] E. R. Szumachowski and H. F. Reid, "Cryogenic toughness of SMA austenitic stainless steel weld metals.–I.–Role of ferrite," *Welding J.*, vol. 57, no. 11, p. 325, 1978.
[9] C. S. Tedmon, D. A. Vermilyea, and J. H. Rosolowski, "Intergranular corrosion of austenitic stainless steel," *J. Electrochem. Soc.*, vol. 118, no. 2, pp. 192–202, 1971.